Electronic Supplementary Material (ESI) for Physical Chemistry Chemical Physics.

ESI: Halogen and Structure Sensitivity of Halobenzene Adsorption on Copper Surfaces †

Christina Schunke*[a], Daniel P. Miller[b], Eva Zurek[c], and Karina Morgenstern[a]

This supplementary information provides LEED pattern and STM images to prove the cleanliness of the surface prior to molecule adsorption. Furthermore, the calibration of the coverage is described based on TPD spectra. The full-range spectra and calculated IR-spectra are presented. The computational details, discussion, figures, and data for DFT calculations performed on fluorobenzene, chlorobenzene, and bromobenzene are provided.

S1 Pristine Surface

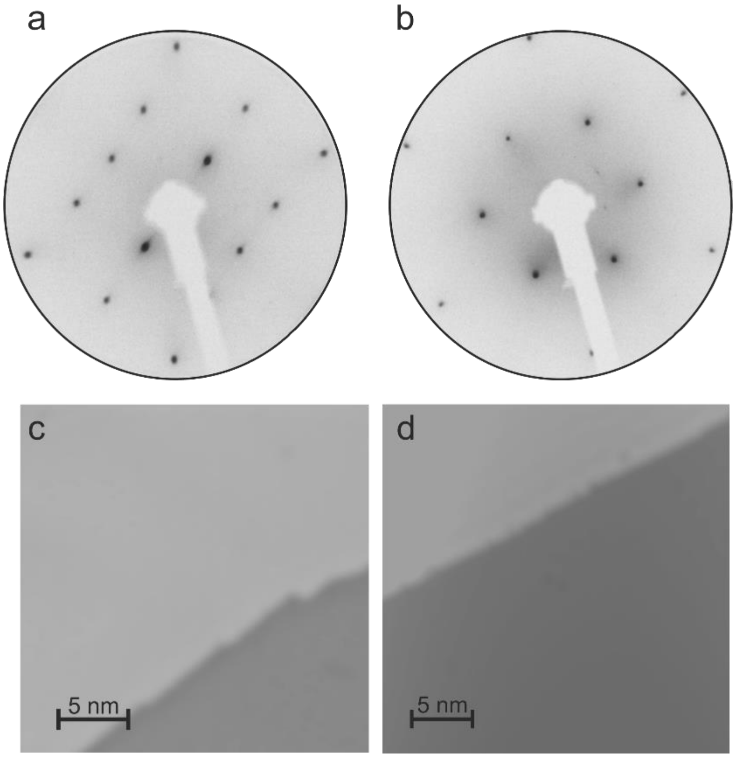

Fig. S1 LEED patterns and STM images of the pristine copper surfaces: (a,b) LEED patterns of the pristine (a) Cu(110) and (b) Cu(111) surface at 298 K on inverted scale. The energy used for the Cu(110) surface was 100 eV (MCP = 0.28 kV) and for the Cu(111) 269 eV (MCP = 0.22 kV). (c,d) STM images of the pristine surfaces of (c) Cu(110) (200 mV, 12 pA) and (d) Cu(111) (-160 mV, 40 pA) both recorded at a temperature between 5 K and 6 K.

---

[a] *Ruhr-Universität Bochum, Lehrstuhl für Physikalische Chemie I, Universitässtraße 150, D-44803 Bochum, Germany.*
[b] *Hofstra University, Department of Chemistry, 106 Berliner Hall, Hempstead, NY 11549, U.S.A.*
[c] *State University of New York at Buffalo, Department of Chemistry, 777 Natural Sciences Complex, Buffalo, NY 14260-3000, U.S.A.*

The copper surfaces were cleaned in all chambers with the same sputtering and annealing cycles as described in the experimental section in the main manuscript.

The LEED patterns were recorded using a LEED spectrometer from OCI (BDL800IR-MCP1-CMX-ISH) (Fig. S1 a,b). The sharp spots of the reciprocal lattice, even at room temperature, suggest a highly ordered thoroughly clean surfaces for both orientations, as supported by STM overview images of the pristine Cu(111) and Cu(110) surfaces (Fig. S1 c,d). No adsorbates are visible on the terraces or at the step-edges.

Both techniques prove that the sputtering and annealing cycles lead to clean surfaces.

S2 Calibration of Surface Coverage

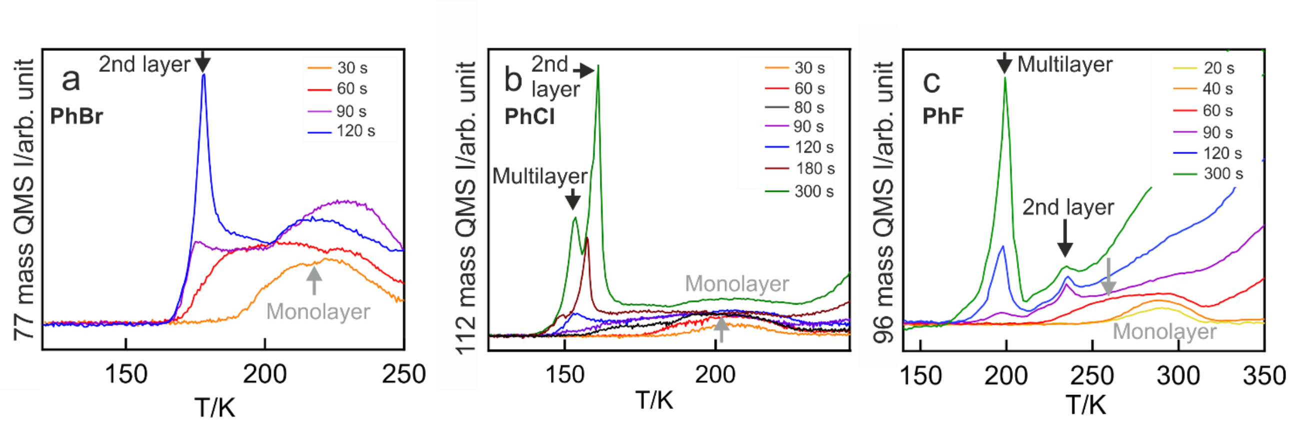

Fig. S2 TPD spectra of (a) bromobenzene (b) chlorobenzene, and (c) fluorobenzene on Cu(111) at different deposition times as marked

The TPD measurements were performed in the IR chamber with a quadrupole mass spectrometer (QMS, *Pfeiffer* PRISMAPLUS® QMG 220™ incl. input/output Modul IO 220). The distance between the mass spectrometer and the sample was around 15 cm. The chamber background was below $5 \cdot 10^{-10}$ mbar. The molecules were adsorbed to the sample cooled by liquid nitrogen to 100 K. The sample was annealed to 350 K by electron bombardment with a heating rate of 0.8 K/s.

The surface temperature was recorded using a thermocouple, spot-welded close to the Cu single crystals.

The deposition time necessary for the deposition of 1 ML was determined through a comparison of the saturation of the broad monolayer peak to literature data[1] (Fig. S2) for deposition times between 30 s and 120 s for bromobenzene, 30 s and 300 s for chlorobenzene, and 20 s and 300 s for fluorobenzene. Thereby, the spectra of all three halobenzenes follow the same trend and only shift in temperature.

At deposition times till (84 ± 5) s, the spectra are dominated by a broad maximum for all three halogenated benzene molecules. The broadenings increase towards lower temperatures with increasing coverage. For chlorobenzene on Ag(111), this broad peak was assigned to 1 ML[1]. At higher coverages sharper additional maxima at 160 K (bromobenzene, chlorobenzene) and 240 K (fluorobenzene) are assigned to the desorption of the second layer. The third peak for even larger deposition times confirms the interpretation. Being for chlorobenzene at 153 K and for fluorobenzene at 200 K, it is assigned to multilayer desorption, following an interpretation of multilayer desorption for benzene molecules[2]. The emergence of the second layer maxima at above 90 s is used to determine the monolayer deposition time. From this, the deposition rate is $(1.2 \pm 0.1) \cdot 10^{-2}$ ML/s, a rate on which the coverage of the IR spectra is based.

S3 Full-range Spectra

In the main manuscript, some not relevant regions of the spectra were not shown for visual clarity. Fig. S3 to Fig. S6 present the full-range RAIR spectra.

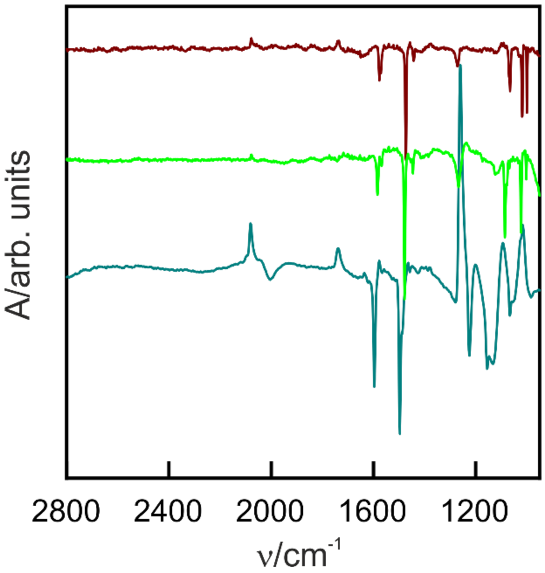

Fig. S3 RAIR spectra of 2 ML bromo-, chloro-, and fluorobenzene on Cu(110). The negative peaks are changes of the background. The intense peak at 2080 cm^{-1} belongs to carbon monoxide molecules in the IR path.

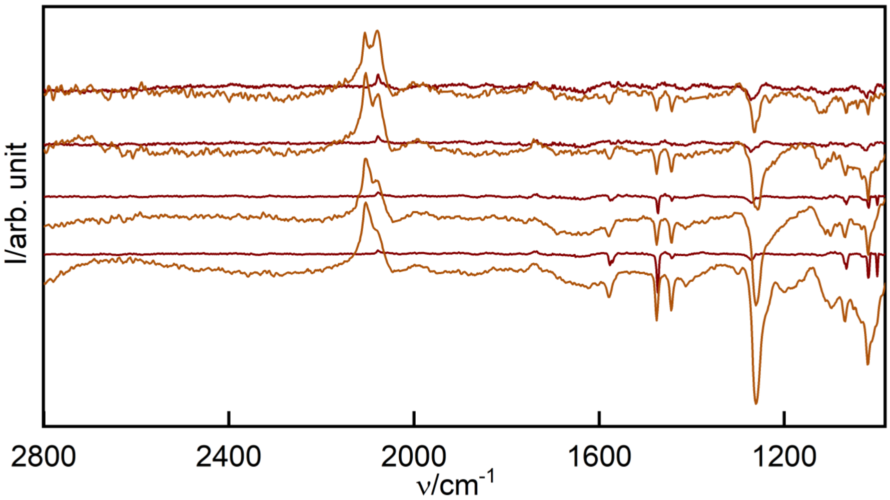

Fig. S4 RAIR spectra of bromobenzene at different coverages (0.25 ML, 0.50 ML, 0.75 ML, 1.00 ML, 1.50 ML) on Cu(111) (darker brown) and Cu(110) (lighter brown): The intense peak at 2080 cm^{-1} corresponds to carbon monoxide molecules. Another artefact is the peak at 1260 cm^{-1}, not considered for the analysis.

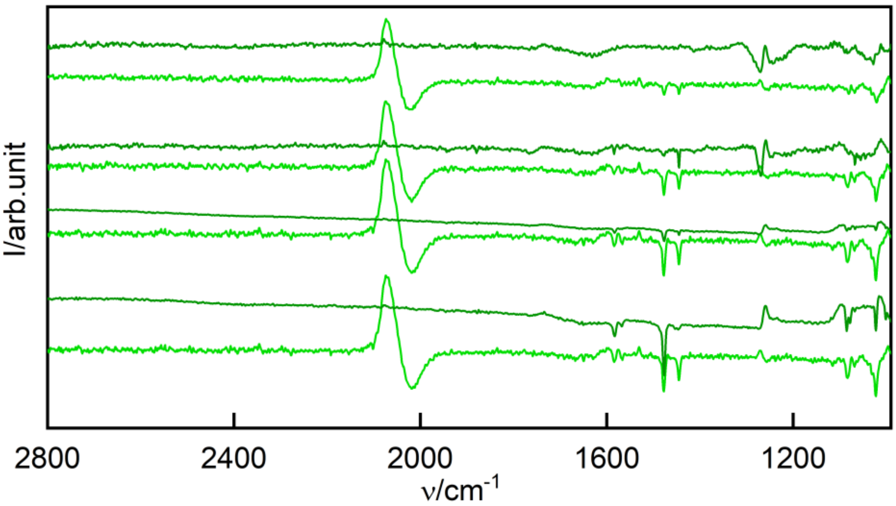

Fig. S5 RAIR spectra of chlorobenzene at different coverages (0.50 ML, 0.75 ML, 1.00 ML, 1.50 ML) on Cu(111) (darker green) and Cu(110) (lighter green): The intense peak at 2080 cm^{-1} correspond to carbon monoxide molecules. Another artefact is the peak at 1260 cm^{-1}, not considered for the analysis.

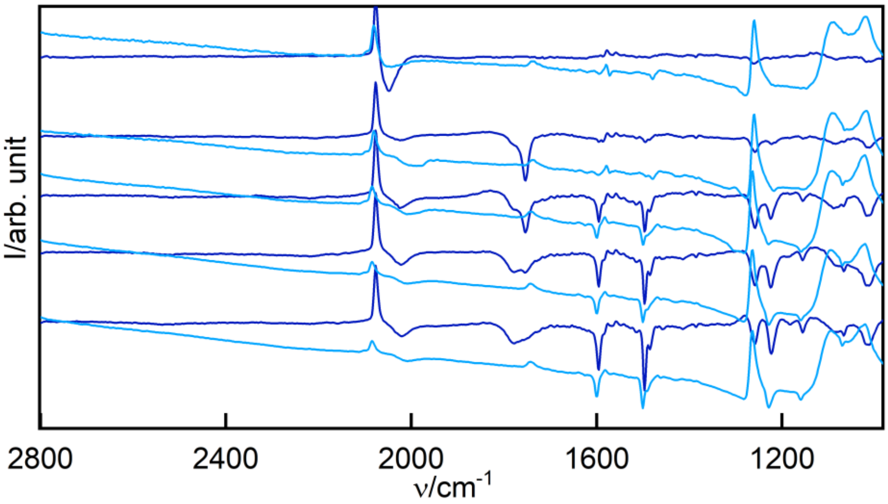

Fig. S6 RAIR spectra of fluorobenzene at different coverages (0.50 ML, 0.75 ML, 1.00 ML, 1.30 ML, 2.00 ML) on Cu(111) (darker blue) and Cu(110) (lighter blue): The intense peak at 2080 cm^{-1} correspond to carbon monoxide molecules. Another artefact is the peak at 1260 cm^{-1}, not considered for the analysis.

S4 DFT Calculations

Computational Details

Molecular dispersion-corrected density functional theory (DFT-D3) calculations were performed with the ADF[3,4,5] software package for obtaining vibrational frequencies. The revPBE (revised Perdew-Burke-Ernzerhof) GGA functional[6,7] was combined with the Grimme3[8] dispersion correction, which is referred to as revPBE-D3 but called DFT-D3 in the discussion for simplicity. The TZP[9] (triple-zeta with one polarization function) basis set and frozen core were used in the bromobenzene, chlorobenzene, and fluorobenzene geometry optimizations, with the Br (4s/4p), Cl (3s/3p), F (2s/2p), C (2s/2p), and H (1s) electrons treated explicitly. The computed vibrational frequencies used for generating IR spectra were produced off of the geometry optimized halobenzenes with analytical second derivatives[10,11,12] for comparison to the experimental RAIRS data. Dimers of each halobenzene were modeled in the gas-phase using the ωB97X-D functional[13] and a 6-31G* basis set with Q-Chem. A halogen bonding model mixed with a single weak hydrogen bond, a weak hydrogen bonding model, and a π-π stacking model were built for each halobenzene and assessed for their binding energies.

Periodic dispersion-corrected density functional theory (DFT-D3) calculations were performed with the VASP[14] software package for obtaining monomer adsorption geometries. The geometry optimizations were performed with revPBE-D3[6,7,8] a plane-wave energy cutoff of 500 eV, a Monkhorst-Pack[15] k-point 3x3x1 set, and the projector augmented wave (PAW)[16,17] method for treating the core states as implemented in VASP. The Cu(111) surface was modeled 4 layers deep, consisted of 120 atoms, and the bottom two layers were kept fixed at the computed revPBE-D3 lattice constant while the top two layers were allowed to relax. The top-down and side views of the adsorption geometries for each halobenzene are given below, with fluorobenzene being most parallel and bromobenzene being the most tilted in respect to the flat surface.

Computational Discussion

To provide further insight into the experimental RAIRS data collected for fluorobenzene, chlorobenzene, and bromobenzene, density functional theory (DFT) calculations were undertaken. In good agreement with experiment's low coverage RAIRS data, it was found that fluorobenzene lies the flattest on Cu(111), chlorobenzene tilts off the parallel adsorption, and bromobenzene tilts the most (Fig. S11 to Fig. S16). This explains why fluorobenzene only displays signals past monolayer coverages while chlorobenzene and bromobenzene display some vibrational signals below full monolayer coverage as RAIRS will display vibrations that are off the parallel to the surface. Another detractor facing fluorobenzene at submonolayer coverages is that fluorobenzene is the least likely of all the halobenzenes to π-π stack and adsorb perpendicular to the surface as shown in Tab. S3. This is due to fluorine being the most deactivating of the halogens and forcing the ring partially negative in charge and thus more repulsive to another fluorobenzene with a similar partial negative charge on the ring. Bromobenzene was shown to be the most prone to π-π stacking and have perpendicular adsorption since bromine has the least impact on the electronic redistribution upon functionalization to the ring, which further explains the easily observed submonolayer signals from bromobenzene (see Tab. S3). Fluorobenzene was also found to bind the strongest through weak hydrogen bonds relative to chlorobenzene and bromobenzene, shown in Tab. S3, and as a result fluorobenzene should prefer side-to-side binding and have a fully flat and interactive monolayer. Chlorobenzene and bromobenzene also have a propensity for side-to-side interactions, shown in Tab. S3, coupled with dispersion forces from the Cu atoms but are not nearly as large in intermolecular side-to-side bindings as fluorobenzene. Chlorobenzene was found to lie intermediate to fluorobenzene and bromobenzene for the aforementioned properties in that chlorobenzene binds favorably to other chlorobenzene molecules all while tilting off parallel adsorption when adsorbed, which supports the identification of signals at submonolayer coverages (see Tab. S3 and Fig. S13 and Fig. S14). Fluorobenzene was found to prefer a hollow binding site for the fluorine atom while chlorobenzene and bromobenzene prefer top binding sites for the chlorine and bromine atoms, which supports the greater tilting in chlorobenzene and bromobenzene further as the chlorine and bromine have to push upward to accommodate the copper interaction. These binding geometries are shown in Fig. S11 to Fig. S16. This is further highlighted by the fluorine binding closest in proximity to the Cu surface while chlorine and bromine adsorb further upward (see Tab. S3). The dimer geometries used for assessing the interaction in fluorobenzene, chlorobenzene, and bromobenzene are shown in Fig. S8 to Fig. S10. See below for data pertaining to the halobenzenes used to make sense of the experimental RAIRS data within the discussion.

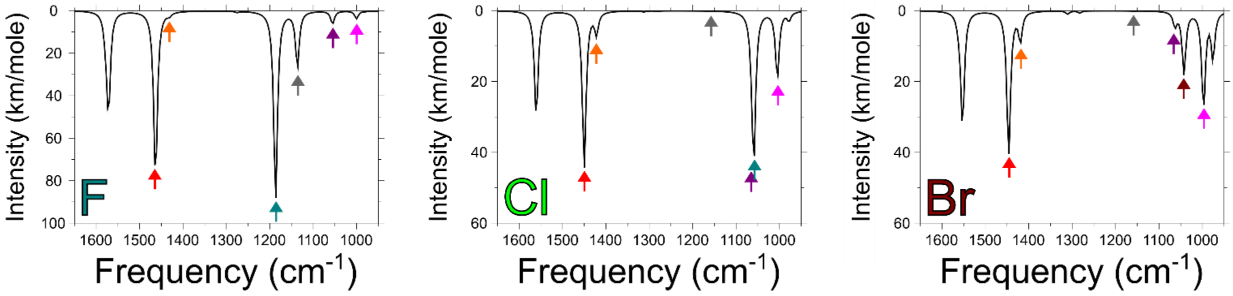

Fig. S7 The DFT-D3 calculated vibrational frequencies, used for simulating the IR spectra, for gas-phase (left) fluorobenzene (F), (middle) chlorobenzene (Cl), and (right) bromobenzene (Br) are shown. Color coordination with the inset arrowheads placed at particular peaks is used to simplify correspondence to experimental peak assignments in the main text for each halobenzene.

Tab. S1 Calculated wave numbers of the vibrational modes of PhBr, PhCl, and PhF using revPBE-D3.

vibration (cm^{-1})	PhBr	PhCl	PhF
ν(C-X)	1042	1059	1187
ν(C-C)	1446	1450	1463
ν(C-C)	1419	1422	1431
β(C-H)	1165	1163	1136
β(C-H)	1063	1064	1055
β(C-H)	997	1005	1000

Tab. S2 Calculated wave numbers of the vibrational modes of PhBr, PhCl, and PhF using ωB97X-D.

vibration (cm^{-1})	PhBr	PhCl	PhF
ν(C-X)	1048	1065	1225
ν(C-C)	1449	1452	1473
ν(C-C)	1417	1419	1430
β(C-H)	1152	1148	1130
β(C-H)	1055	1054	1048
β(C-H)	999	1001	998

Tab. S3 The halogen bonding/weak hydrogen bonding, weak hydrogen bonding, and π-π stacking dimer binding energies (kJ/mol) are given. The distance, d_{int}, between the halogens (X—X) in the halogen bonding and hydrogens to halogens (X—H) in the weak hydrogen bonding for the halogen/weak hydrogen bonding model are displayed. The hydrogens to the halogens (X—H) distance and π-π stacking distance are shown as d_{int} for the weak hydrogen bonding and π-π stacking dimer models. The adsorption angle, α, and the distance between the halogens and the Cu surface, d_x, are given to the right of the table for each halobenzene. The interacting dimers for each halobenzene are shown in Fig. S8 to Fig. S10.

Fluorobenzene				
	BE (kJ/mol)	d_{int} (nm)	α (°)	d_x (nm)
Halogen/Weak Hydrogen Bonding	7.52	0.33/0.24		
Weak Hydrogen Bonding	17.93	0.24		
π-π stacking	23.10	0.33		
Cu—F			92	0.28
Chlorobenzene				
	BE (kJ/mol)	d_{int} (nm)	α (°)	d_x (nm)
Halogen/Weak Hydrogen Bonding	4.48	0.38/0.30		
Weak Hydrogen Bonding	10.21	0.29		
π-π stacking	26.94	0.34		
Cu—Cl			94	0.30
Bromobenzene				
	BE (kJ/mol)	d_{int} (nm)	α (°)	d_x (nm)
Halogen/Weak Hydrogen Bonding	6.44	0.40/0.30		
Weak Hydrogen Bonding	10.72	0.31		
π-π stacking	29.98	0.34		
Cu—Br			95	0.31

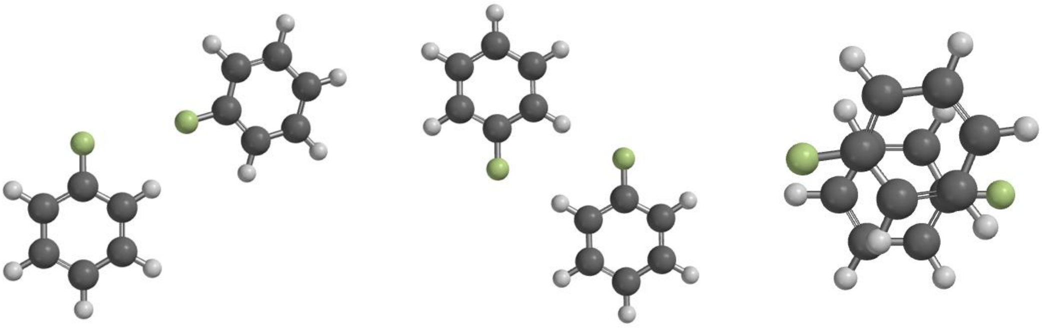

Fig. S8: (Left) Halogen Bonding/Weak Hydrogen Bonding Model, (Middle) Two Weak Hydrogen Bonding Model, (Right) π-π Stacking Model for Fluorobenzene.

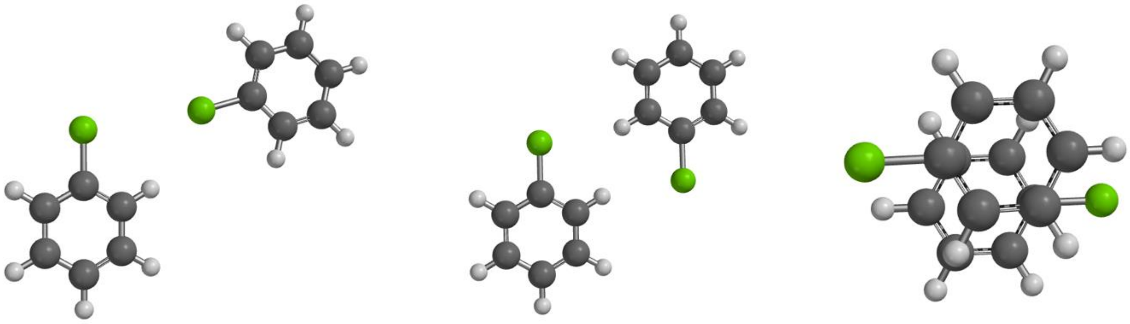

Fig. S9: (Left) Halogen Bonding/Weak Hydrogen Bonding Model, (Middle) Two Weak Hydrogen Bonding Model, (Right) π-π Stacking Model for Chlorobenzene.

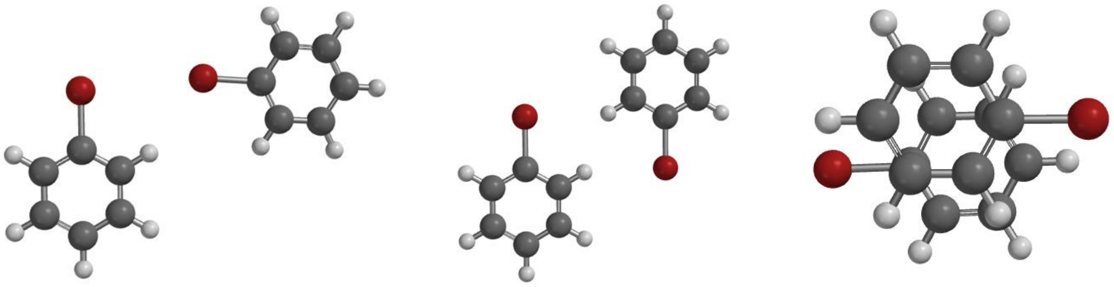

Fig. S10: (Left) Halogen Bonding/Weak Hydrogen Bonding Model, (Middle) Two Weak Hydrogen Bonding Model, (Right) π-π Stacking Model for Bromobenzene.

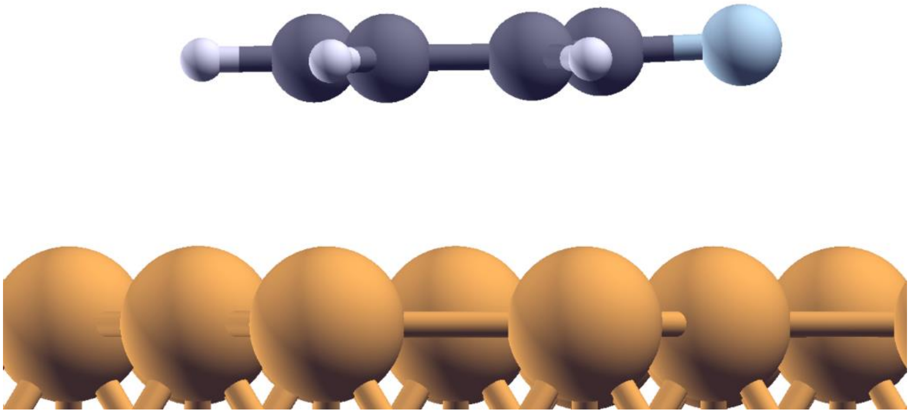

Fig. S11: The side view of the adsorption geometry of fluorobenzene to Cu(111). Note the near parallel adsorption of the molecule with respect to the surface.

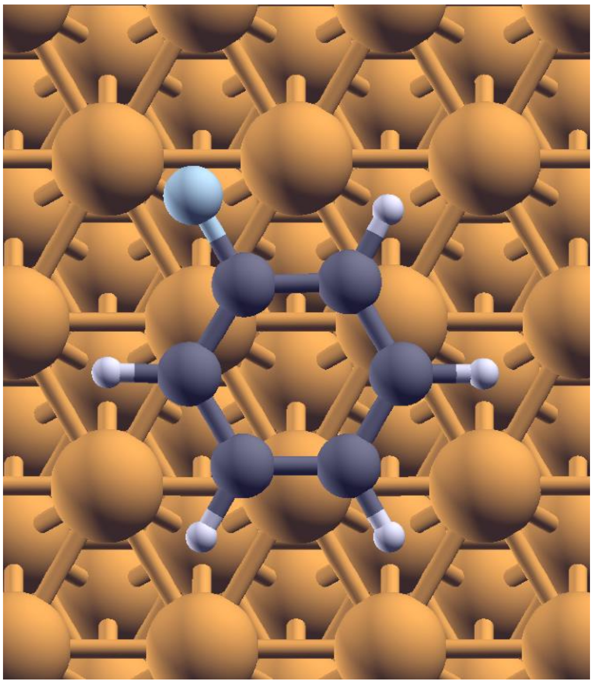

Fig. S12: The top-down view of the adsorption geometry of fluorobenzene to Cu(111). The fluorine prefers lying above a H_{hcp} binding site.

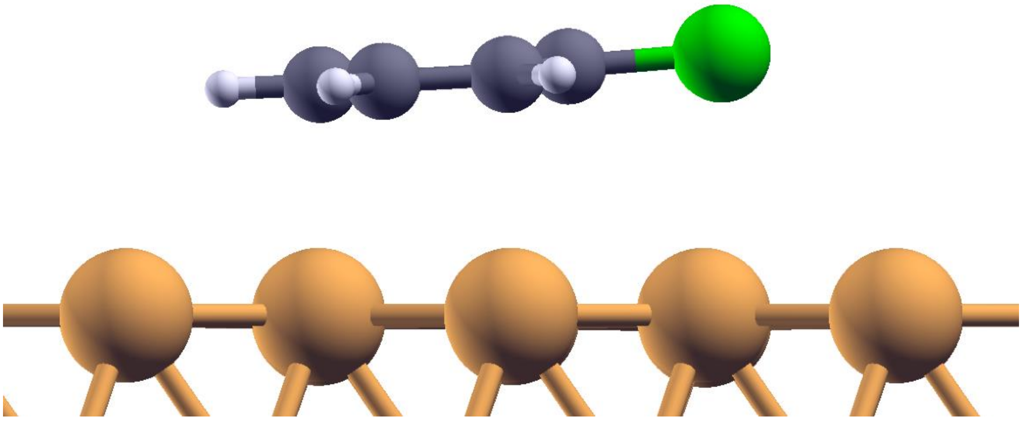

Fig. S13: The side view of the adsorption geometry of chlorobenzene to Cu(111). Note the tilted adsorption of the molecule with respect to the surface.

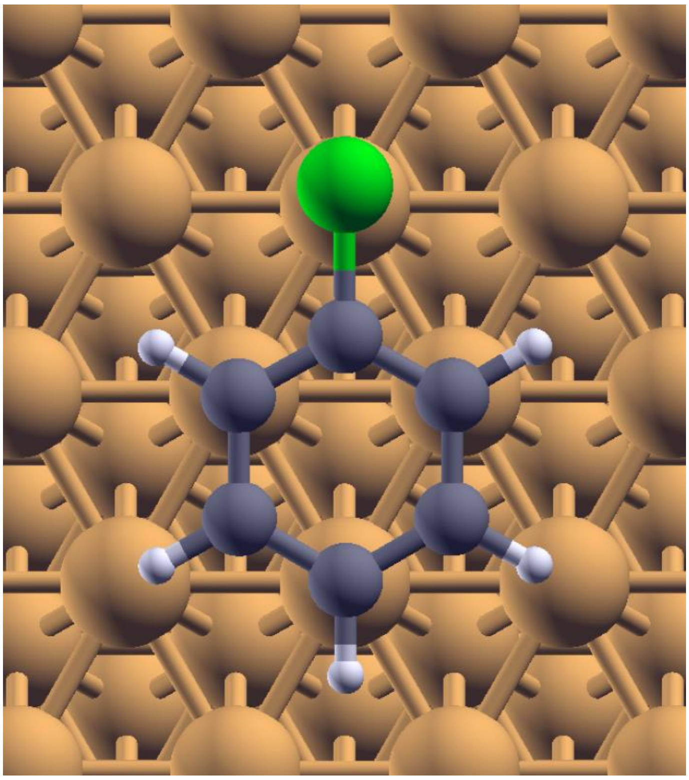

Fig. S14: The top-down view of the adsorption geometry of chlorobenzene to Cu(111). The chlorine prefers lying above a T binding site.

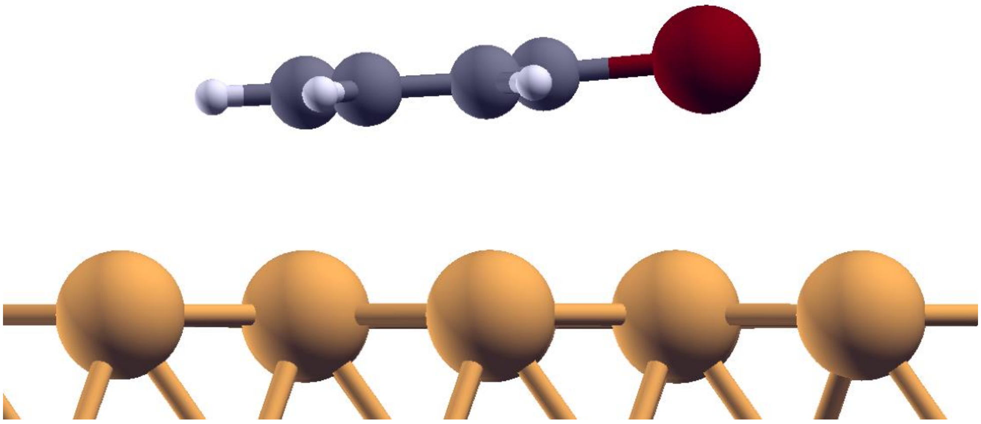

Fig. S15: The side view of the adsorption geometry of bromobenzene to Cu(111). Note the tilted adsorption of the molecule with respect to the surface.

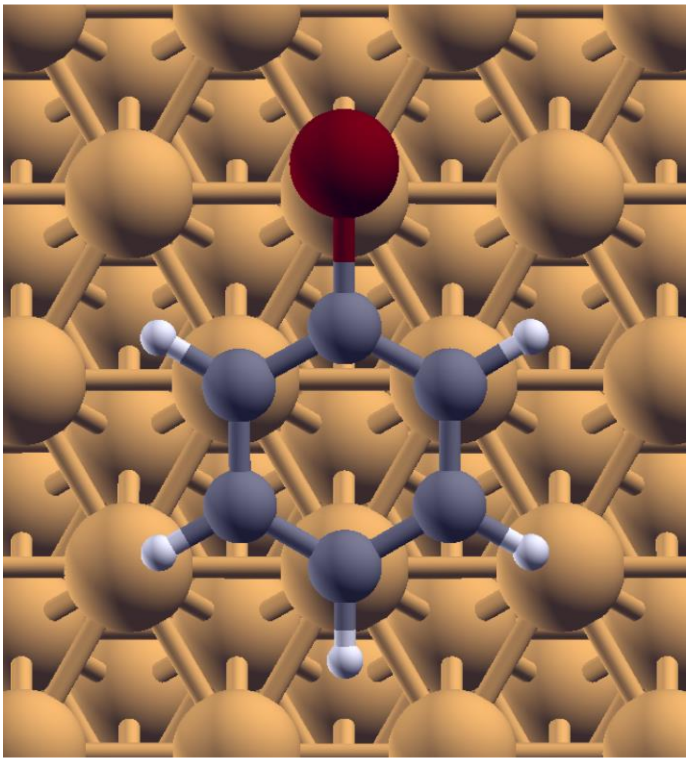

Fig. S16: The top-down view of the adsorption geometry of bromobenzene to Cu(111). The bromine prefers lying above a T binding site.

Notes and references

1 X.-L., Zhou and J.M. White, *J. Chem. Phys.,* 1990, **92**, 5612-5621.
2 M. Xi, M.X. Yang, S.K. Jo, B.E. Bent and P. Stevens, *J. Chem. Phys*., 1994, **101**, 9122-9131.
3 G. te Velde, F. M. Bickelhaupt, S. J. A. van Gisbergen, C. Fonseca Guerra, E. J. Baerends, J. G. Snijders, T. Ziegler, *J. Comp. Chem*., 2001, **22**, 931.
4 C. Fonseca Guerra, J. G. Snijders, G. te Velde, E. J. Baerends, *Theor. Chem. Acc.*, 1998, **99**, 391.
5 ADF2013, SCM, Theoretical Chemistry, Vrije Universiteit, Amsterdam, The Netherlands, http://www.scm.com
6 J. P. Perdew, K. Burke, M. Ernzerhof, *Phys. Rev. Lett.*, 1996, **77**, 3865.
7 Y. Zhang, W. Yang, *Phys. Rev. Lett.*, 1998, **80**, 890.
8 S. Grimme, J. Antony, S. Ehrlich, H. Krieg, *J. Chem. Phys.*, 2010, **132**, 154104.
9 E. van Lenthe, E. J. Baerends, *J. Comp. Chem.*, 2003, **24**, 1142.
10 A. Bérces, R. M. Dickson, L. Fan, H. Jacobsen, D. Swerhone and T. Ziegler, *Comp. Phys. Comm.*, 1997, **100**, 247.
11 H. Jacobsen, A. Bérces, D. Swerhone and T. Ziegler, *Comp. Phys. Comm.*, 1997, **100**, 263.
12 S. K. Wolff, *Int. J. Quant. Chem.*, 2005, **104**, 645.
13 M. Seth, T. Ziegler, *J.Chem.Theory.Comput., 2012,* **8**, 901.
14 G. Kresse, J. Furthmüller, *Phys. Rev. B*, 1996, **54**, 11169.
15 H. J. Monkhorst, J. D. Pack, *Phys. Rev. B*, 1976, **13**, 5188.
16 P. E. Blöchl, *Phys. Rev. B*, 1994, **50**, 17953.
17 G. Kresse, J. Joubert, *Phys. Rev. B*, 1999, **59**, 1758.